

# **PREFIRE Data User Guide**

## Level 2B Atmospheric Properties (2B-ATM)

Version R01  
(20250430)

Aronne Merrelli  
Nathaniel Miller  
Erin Hokanson Wagner  
Tim Michaels

## Table of Contents

<b>1</b>	<b><i>Introduction</i></b> .....	<b>3</b>
<b>1.1</b>	<b>Mission Overview</b> .....	<b>3</b>
<b>1.2</b>	<b>Data Overview</b> .....	<b>4</b>
1.2.1	Spatial characteristics .....	4
<b>1.3</b>	<b>Purpose</b> .....	<b>6</b>
<b>2</b>	<b><i>Product Description</i></b> .....	<b>6</b>
<b>2.1</b>	<b>Algorithm description</b> .....	<b>6</b>
<b>2.2</b>	<b>File Specifications</b> .....	<b>6</b>
2.2.1	File naming convention .....	6
2.2.2	File format .....	7
2.2.3	Quality flag and bitflags conventions.....	7
2.2.4	Variables.....	8
2.2.5	Variable dimensions .....	9
<b>3</b>	<b><i>Updates Since Previous Version</i></b> .....	<b>14</b>
<b>4</b>	<b><i>Known Issues</i></b> .....	<b>14</b>
<b>5</b>	<b><i>Resources</i></b> .....	<b>16</b>
<b>6</b>	<b><i>References</i></b> .....	<b>16</b>

# 1 Introduction

This user guide contains information for the PREFIRE data collections PREFIRE\_SAT1\_2B-ATM and PREFIRE\_SAT2\_2B-ATM, which are archived by the Atmospheric Science Data Center (ASDC) at the NASA Langley Research Center. These collections contain clear-sky atmospheric properties as derived from spectral radiance data collected by the PREFIRE Thermal Infrared Spectrometers (PREFIRE-TIRS).

## 1.1 Mission Overview

The Science Mission Directorate (SMD) at NASA Headquarters selected the Polar Radiant Energy in the Far InfraRed Experiment (PREFIRE) as an Earth System Science Pathfinder (ESSP) Earth Venture Instrument (EVI-4) class Mission of Opportunity. Through spectrally resolved observations of radiances spanning the radiatively significant portions of the Mid- and Far-InfraRed (MIR and FIR), PREFIRE addresses two complementary hypotheses:

1. Time-varying errors in both FIR surface emissivity and thermal radiation modulate estimates of energy exchanges between the surface and the atmosphere in the Arctic.
2. These terms are responsible for a large fraction of the spread in projected rates of change for Arctic surface, ocean, and atmosphere characteristics.

These hypotheses are addressed through five related objectives:

- O1.1 Quantify snow and ice FIR emissivity spectra and their variability on seasonal scales;
- O1.2 Quantify the FIR thermal radiation and its response to seasonal variations in cloud cover / water vapor;
- O1.3 Quantify variability in Arctic spectral surface emission and the thermal radiation across the FIR owing to transient cloud and water vapor and sub-daily surface phase-change processes;
- O2.2 Quantify thermal emission errors on projected rates of Arctic warming and sea ice loss;
- O2.3 Determine the impact of improved surface emissivity on modeled ice sheet dynamic processes on hourly scales.

PREFIRE uses broadband infrared (> 75% of surface emitted thermal radiation) radiance measurements made from the separate orbiting platforms (CubeSats) to address the science objectives. The PREFIRE payloads are two stand-alone instruments built at JPL using heritage from the Mars Climate Sounder and the Moon Mineralogy Mapper. The PREFIRE instruments are thermal infrared imaging spectro-radiometers with more than 50 spectral bands. Each PREFIRE instrument uses ambient temperature thermopile detectors and operates in a pushbroom mode with a point and stare mirror for viewing nadir (Earth), space, and a calibration target. PREFIRE data are calibrated with data from views of the internal calibration target and of space, which are viewed multiple times per orbit.

Soon after launch, the orbit altitude was approximately 531 km for both satellites. However, the PREFIRE CubeSats do not have station-keeping abilities and so their altitudes decrease with time. The current satellite altitude is recorded within the Atmospheric Properties (2B-ATM) data product files as the *sat\_altitude* field (in the *Geometry* data group).

The PREFIRE project delivers space-based measurements of radiative fluxes, cloud masks, spectrally variant surface emissivity ( $\epsilon_\lambda$ ), and column water vapor (CWV). These are science products with the precision, resolution, and coverage needed to improve our understanding of polar energy balances and Earth system effects over diurnal and seasonal cycles at scales that capture surface and cloud variability. During its approximately one-year baseline mission, PREFIRE will capture the natural variability in Arctic and Antarctic CWV and surface temperature. PREFIRE reduces uncertainties in the surface and

atmospheric components of the polar energy budget.

## 1.2 Data Overview

The PREFIRE 2B-ATM product contains output from the 2B-ATM clear-sky atmospheric profile retrieval algorithm. The primary output variable is the total column water vapor (CWV). Additional retrieval variables are temperature profiles, water vapor profiles, and surface temperature.

As 2B-ATM is a clear-sky retrieval algorithm, it is run on those PREFIRE-TIRS observations that are identified as "clear" or "likely clear" by the PREFIRE Cloud Mask (2B-MSK) retrieval. Thus, users should expect the output to exist only according to those spatial regions.

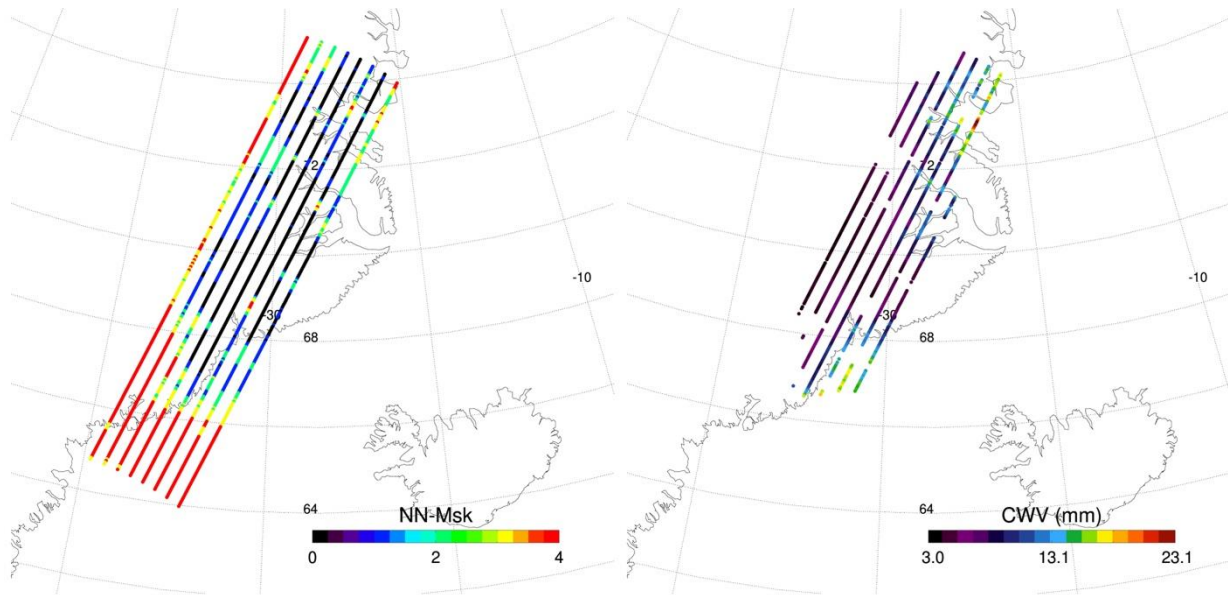


Figure 1-1. A segment of SAT2 granule ID 00659 (2024-07-07): the 2B-MSK cloud categories (left) and the retrieved CWV (right). This example region illustrates the coverage that might be expected in the 2B-ATM product. In early testing, roughly 25% of the available polar data is retrieved and represented in the 2B-ATM product.

### 1.2.1 Spatial characteristics

The PREFIRE-TIRS instruments collect data continuously in a pushbroom mode, with an integration time of 0.7 seconds for each data frame. Each data frame contains a spectral measurement from each cross-track scene collected simultaneously. Within this continuous data collection, there are planned interruptions due to calibration cycles or data downlinks, and there are also occasional interruptions due to unplanned instrument operations changes or outages. Each calibration cycle takes ~18.7 seconds for PREFIRE-TIRS-1 and ~9.7 seconds for PREFIRE-TIRS2, which implies a gap of approximately 27 and 14 data frames, respectively. Data downlinks create data gaps of up to 13 minutes, and the exact length varies.

Within the orbital swath there are eight distinct tracks of data associated with the eight separate spatial scenes for each PREFIRE-TIRS. The approximate scene footprint sizes are 11.8 km x 34.8 km (cross-

track x along-track), with gaps between each scene of approximately 24.2 km. The swath itself is ~264 km across. Note that the scene footprint and swath sizes quoted here are for the orbit altitude soon after launch. However, the footprint size will slowly become smaller as the orbit altitude decreases with time. Do not assume constant footprint or swath dimensions.

PREFIRE-TIRS spatial footprints overlap each other in the along-track dimension. Assuming that no data are missing, any given point along the orbit swath will be observed by up to about 7 overlapping footprints in the along-track direction. The number of footprints that overlap a given footprint will slowly become smaller during the mission, as the satellites' orbital altitudes decrease. Do not assume an integer number of overlapping footprints.

A single data file or granule consists of data collected during approximately one orbit, beginning and ending near the equator to avoid granule borders over the polar regions. Data files are NetCDF4 format. Because the amount of retrieval output depends on the clear-sky fraction, the file size varies and can be in the range of 4-9 MB in size. These data collections are archived at the ASDC DAAC and can be found at [https://asdc.larc.nasa.gov/project/PREFIRE/PREFIRE\\_SAT1\\_2B-ATM\\_R01](https://asdc.larc.nasa.gov/project/PREFIRE/PREFIRE_SAT1_2B-ATM_R01) and [https://asdc.larc.nasa.gov/project/PREFIRE/PREFIRE\\_SAT2\\_2B-ATM\\_R01](https://asdc.larc.nasa.gov/project/PREFIRE/PREFIRE_SAT2_2B-ATM_R01).

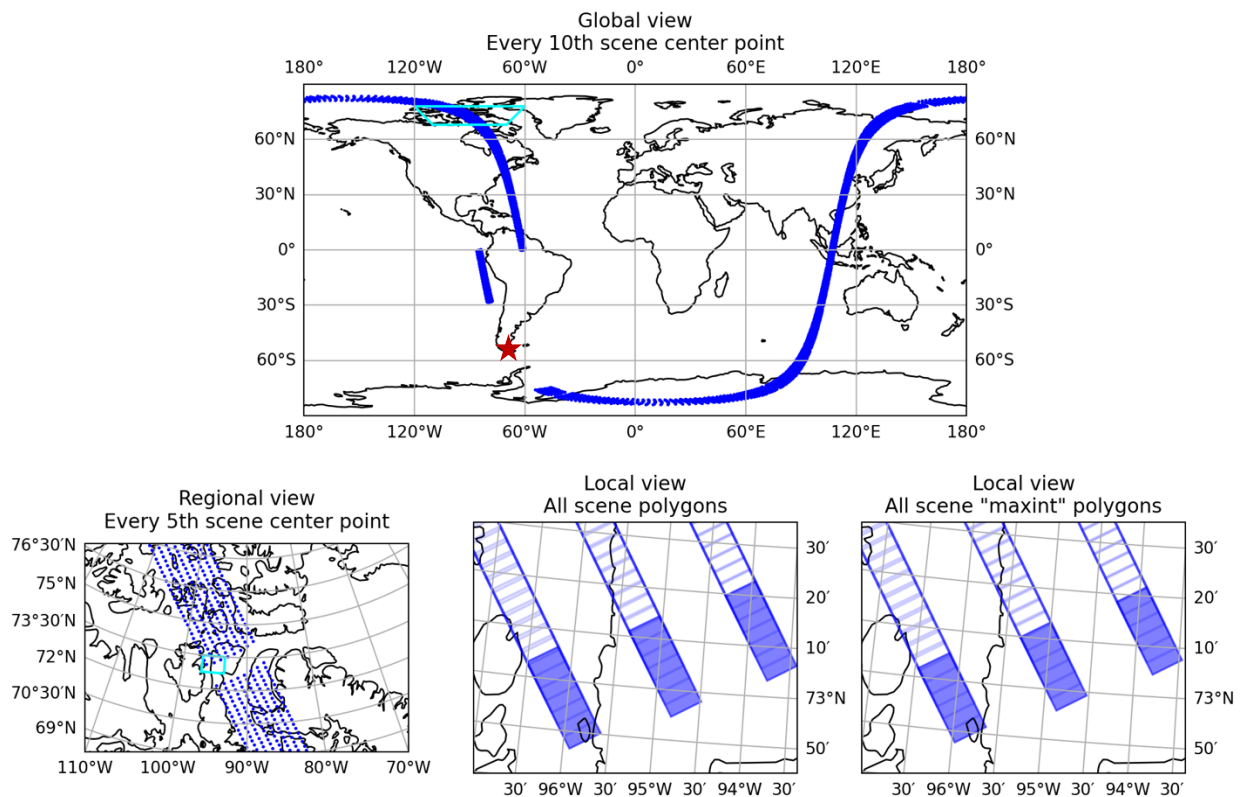


Figure 1-2. An example geolocated orbit (top panel) and focused regional and local plots (bottom panels). The global plot was selected to illustrate a data gap due to a data downlink at the Punta Arenas, Chile ground station, from approximately -70°S to -30°S on the ascending pass at the end of the granule. The zoomed in regional view (lower left) shows the data within the small cyan box in the global plot, and illustrates a smaller data gap due to instrument calibration. The local views (lower middle and right) show the actual scene ground footprint polygons, for the cyan box denoted in the regional view. The

first scene’s polygon is filled blue, to illustrate the shape of the full field of view (FOV) for one data integration. During the 0.7 second integration time, the satellite moves along track slightly more than 5 km, which means the leading and trailing edges of the instantaneous FOV have translated forward by the same amount. The lower right plot shows the “max integration” footprint polygon, which includes the interior portion of the scene footprint that was within the sensor field of view for the entire integration period.

### 1.3 Purpose

The primary output of the 2B-ATM retrieval is the vertically integrated water vapor amount, reported as the Column Water Vapor (CWV). The 2B-ATM product can be used to quantify the water vapor amount within the PREFIRE-TIRS observation footprints, which controls various radiative properties of the atmospheric column such as the vertical longwave flux profile and radiative heating and cooling profiles.

## 2 Product Description

### 2.1 Algorithm description

The 2B-ATM algorithm uses an optimal estimation (OE) solver to retrieve an estimate of the clear-sky temperature profiles, water vapor profiles, and surface temperature. It uses the AUX-MET and Surface Emissivity (2B-SFC) products for prior information about the atmospheric profile and surface spectral emissivity, respectively. The algorithm generally follows the optimal estimation formalism of Rodgers (2000), and the specific implementation closely follows the OE solver used in the NASA OCO-2 Level 2 retrieval algorithm (Crisp 2021). The Principal Component-based Radiative Transfer Model (PCRTM) is used as the forward radiance model (Liu 2006). The state vector is composed of surface temperature and the thermodynamic (temperature and water vapor) profile. The surface emissivity is held constant to the 2B-SFC retrieved spectral surface emissivity, or a constant value of 1.0 if the 2B-SFC retrieval is not available. Because the information in the PREFIRE-TIRS spectral measurements is limited, the 101-level vertical grid in the native PCRTM output files is combined into a set of 7 coarser layers. The main retrieval output is the column water vapor (CWV), which is the vertical integral of the water vapor profile.

During testing for the R01 data product release, residual radiance biases were noted in the 1B-RAD product that in turn caused significant bias and scatter in the 2B-ATM OE algorithm output data. To mitigate biases in the 2B-ATM output, an empirical radiance bias correction was implemented in the R01 2B-ATM data product release for SAT2. A similar empirical radiance bias correction for SAT1 2B-ATM will be implemented in the next 2B-ATM data product release.

Further detail about the 2B-ATM algorithm can be found in the associated Algorithm Theoretical Basis Document (ATBD).

### 2.2 File Specifications

#### 2.2.1 File naming convention

File names for this collection follow the following convention:

```
PREFIRE_SAT<satID>_<productID>_<collectionVersion>_<internalProductVersion>  
> <YYYYMMDDhhmmss>_<granuleID>.nc
```

For example, a representative Level 2B Atmospheric Properties (2B-ATM) product granule collected by PREFIRE-SAT1 on June 1, 2024 would have the following filename:

PREFIRE\_SAT1\_2B-ATM\_R01\_P00\_20240601185321\_00123.nc

### 2.2.2 File format

PREFIRE 2B-ATM data product files are created in NetCDF4 format with standard metadata. These files can be read with standard NetCDF libraries available in all popular scripting languages and many data visualization programs.

### 2.2.3 Quality flag and bitflags conventions

A quality assessment flag is given in the output, which specifies the state of the iterative retrieval algorithm. The values of *atm\_quality\_flag* (in the *Atm* data group) are given in Table 2-1. The best quality data has a flag value of 0. Retrievals with a flag value of 1 could have usable results, but users should treat these data with caution as the quality assessment check indicates these values have poorer precision and accuracy. A flag value of 2 indicates that the retrieval did not converge, which means the data should be ignored since the iterative algorithm may have halted in an unpredictable state. Observations skipped by the retrieval (due to the cloud mask, for example) will contain the netCDF defined Fill Value (-99) for the quality flag.

Table 2--1. QA flag descriptions

<i>atm_quality_flag</i> value	Description
0	Good retrieval
1	Retrieval converged but did not meet quality check
2	Retrieval did not converge

The current quality check for the R01 2B-ATM product is a threshold on the reduced  $\chi^2$  (less than 5) and iteration count (less than 3).

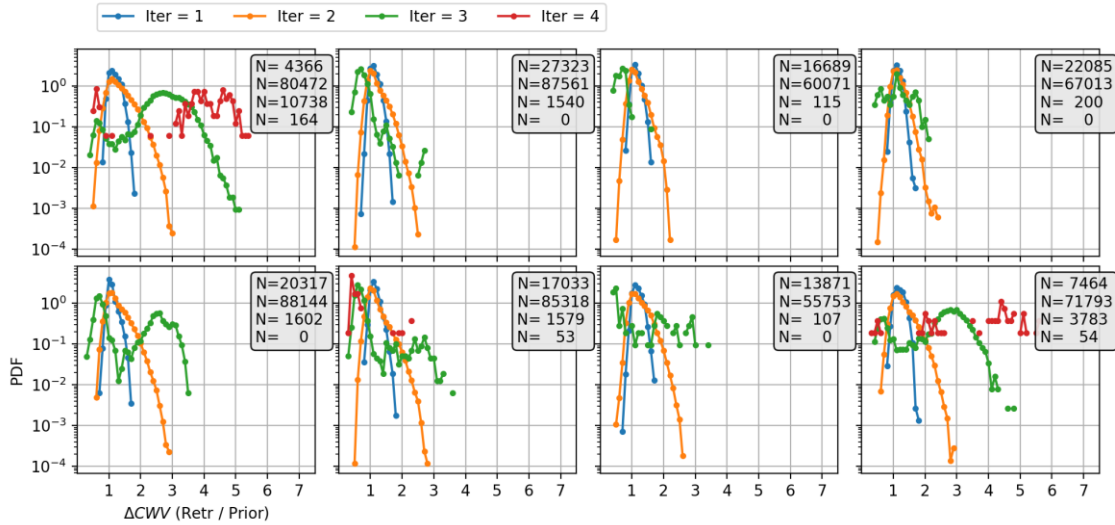


Figure 2-1. The PDF of CWV ratio (retrieved CWV divided by the CWV prior mean) as a function of retrieval iteration evaluated for R01 test data.

In Figure 2-1, the distribution of CWV ratio for iterations 3 and 4 shows markedly increased scatter, particular to ranges of high CWV – factors of 2 - 5 larger than the prior mean value. Such large values of CWV are more likely to be retrieval errors than actual high values of CWV. Our current hypothesis is that these retrievals are affected by thin cloud contamination, and they tend to have higher values of cloud probability from the 2B-MSK product. Therefore, in the R01 2B-ATM release we decided to include iteration count < 3 as part of the internal quality check.

In most cases the quality flag should be sufficient for identifying the best retrieval output. Understanding the reasons why certain retrievals are marked as low quality, or are missing in the product, requires interrogating the individual bits in *atm\_qc\_bitflags* (in the *Atm* data group). Table 2-2 describes the specific bit flags found in this product.

Table 2--2. QC bit flag descriptions

<i>atm_qc_bitflags</i> bit index	Description
0	Reduced $\chi^2$ is over quality check threshold
1	Failed to converge due to exceeding iteration limit
2	Failed to converge due to exceeding diverging step limit
3	State variable went out of range
4	Solver crashed
5	Retrieval assumed constant blackbody emissivity ( $\epsilon=1$ )
10	No retrieval attempted, due to 2B-MSK
11	No retrieval attempted, due to latitude constraint
12	No retrieval attempted, due to bad 1B-RAD status

## 2.2.4 Variables

The variable specifications for this collection are described below, with one table devoted to each top-level data group in the NetCDF4 file: *Geometry*, and *Atm*. Note that the *Geometry* group, including all variables, is propagated to every downstream Level 2 data product from the Level 1B Radiance product (1B-RAD).

### 2.2.5 Variable dimensions

A summary of all array dimensions is given in Table 2-3. The *xtrack* dimension is equal to the number of cross-track scenes (8, for both instruments), the *spectral* dimension is equal to the number of spectral channels (63 for both instruments), and the *atrack* dimension is equal to the number of along-track Earth observation data frames in the product. The number of along-track frames varies from orbit to orbit, depending on the timing of downlink contacts, calibration data, and other rarer events. Generally, the maximum is around 7700–7900 frames in one product file, with substantially fewer in granules containing downlinks or unplanned instrument/spacecraft events. The additional dimensions *layers* and *levels* contain the vertical dimensions associated with the profile retrievals. In the current versions of the retrieval, these are output on a set of 7 fixed pressure layers (*layers* = 7 and *levels* = 8). The *state* dimension refers to the dimension of the state vector, which is currently equal to 15, for the surface temperature and the temperature and water vapor profiles.

Table 2-3

<b>Dimension</b>	<b>Abbreviation</b>
Along-track	<i>atrack</i>
Cross-track	<i>xtrack</i>
Number of channels	<i>spectral</i> (= 63)
Number of Layers	<i>nlayers</i> (= 7)
Number of Levels	<i>nlevels</i> (= 8)
State Vector 1	<i>statev1</i> (= 15)
State Vector 2	<i>statev2</i> (= 15)
UTC parts	<i>UTC_parts</i> (= 7)
FOV (footprint) vertices	<i>FOV_vertices</i> (= 4)
<b>Dimension label</b>	<b>Definition (C-order)</b>
1D	( <i>atrack</i> )
1Dx	( <i>xtrack</i> )
2D	( <i>atrack, xtrack</i> )
2Dp	( <i>atrack, spectral</i> )
2Du	( <i>atrack, UTC_parts</i> )
3D	( <i>atrack, xtrack, spectral</i> )
3Dv	( <i>atrack, xtrack, FOV_vertices</i> )
3Dn	( <i>atrack, xtrack, layers</i> )
3Dm	( <i>atrack, xtrack, levels</i> )
4D	( <i>atrack, xtrack, statev1, statev2</i> )

### 2.2.5.1 Geometry group

The *Geometry* data group consists of all timing, observation geometry, and geolocation variables produced during Level-1B processing (see Table 2-4). This data group and its contents will be replicated within any relevant downstream product (e.g., Level 2 data products), rather than stored as a separate geometry file.

Users of NetCDF software packages that try to automatically decode times should be aware that these packages may incorrectly interpret the *ctime* variable as a UTC time. The *ctime* variable is a count of total fractional SI seconds since the epoch 2000-01-01T00:00:00 UTC (i.e., no leap second adjustments since that epoch), while the UTC time standard is adjusted to account for all leap seconds. For example, when the PREFIRE *Geometry* group is read by the `open_dataset` function of the Python `xarray` package using the default `decode_times=True` argument, the resulting *ctime* values (with `datetime64` data type) will differ from the *time.UTC\_values* variable by the number of leap seconds that occurred between 2000-01-01T00:00:00 UTC and the observation time. Users of `xarray` and other packages that exhibit this behavior are recommended to use *ctime* along with *ctime\_minus.UTC* to calculate UTC times if desired, and/or consult *time.UTC\_values* to verify the correct UTC timestamps of PREFIRE observations.

For example, for an `xarray` dataset, a `datetime64` `DataArray` could be computed as follows:

```
import xarray as xr
ds = xr.open_dataset({path to 1B-RAD product}, group='Geometry')
ds['UTC_dt64'] = ds['ctime'] - ds['ctime_minus.UTC']
```

Further details on the handling of leap seconds in the Climate and Forecast (CF) NetCDF Metadata Conventions can be found in Section 4.4.1 of the CF-1.9 Conventions: <https://cfconventions.org/Data/cf-conventions/cf-conventions-1.9/cf-conventions.html#calendar>.

Table 2--3

Variable Name	Type	Dimension	Units	Description
obs_ID	int64	2D		unique integer identifier for each TIRS look YYYYMMDDhhmmssb, composed of UTC date (YYYYMMDD) and time (hhmmss) at TIRS image integration midpoint, t = tenths of seconds [0–9], b = satellite number [1–2],

				d = scene number [1–8]
ctime	float64	1D	seconds	continuous time since the epoch 2000-01-01T00:00:00 UTC (i.e., similar to TAI) at the midpoint of each TIRS image integration
ctime_minus_UTC	int8	1D	seconds	continuous time minus UTC (i.e., leap seconds since the ctime epoch) at the midpoint of each TIRS image integration
time_UTC_values	int16	2Du	various	UTC datetime at the midpoint of each TIRS image integration, represented as an integer array. Array parts: year, month, day, hour, minute, second, millisecond
latitude	float32	2D	degrees_north	topography-corrected latitude of FOV centroid
longitude	float32	2D	degrees_east	topography-corrected longitude of FOV centroid
vertex_latitude	float32	3Dv	degrees_north	topography-corrected latitude for each of the four vertices/corners (arranged counterclockwise starting at the trailing-left corner) of a 4-sided polygon that closely approximates the geolocated FOV (orbital motion taken into account)
vertex_longitude	float32	3Dv	degrees_east	topography-corrected longitude for each of the four vertices/corners (arranged counterclockwise starting at the trailing-left corner) of a 4-sided polygon that closely approximates the geolocated FOV (orbital motion taken into account)
land_fraction	float32	2D		land_area / total_area (remainder is water_area) within the FOV, according to the Digital Elevation Model (DEM)
elevation	float32	2D	m	mean topographic elevation within the FOV
elevation_stdev	float32	2D	m	standard deviation of topographic elevation within the FOV
viewing_zenith_angle	float32	2D	degrees	viewing zenith angle at the FOV centroid
viewing_azimuth_angle	float32	2D	degrees	viewing azimuth angle at the FOV centroid (zero is north, clockwise-positive looking down from the zenith)
solar_zenith_angle	float32	2D	degrees	solar zenith angle at the FOV centroid
solar_azimuth_angle	float32	2D	degrees	solar azimuth angle at the FOV centroid (zero is north, clockwise-positive looking down from the zenith)
solar_distance	float64	2D	km	distance from FOV centroid to the solar barycenter
subsat_latitude	float32	1D	degrees_north	sub-satellite latitude

subsat_longitude	float32	1D	degrees_east	sub-satellite longitude
sat_altitude	float32	1D	km	satellite altitude above the reference ellipsoid (at the sub-satellite point)
sat_solar_illumination_flag	int8	1D		flag specifying whether the spacecraft is illuminated by the sun; 0=no, 1=partial, 2=full
geoloc_quality_bitflags	uint16	2D		integer composed of bit flags that contain info about the quality of the overall geolocation of each along-track frame of scenes
maxintgz_verts_lat	float32	3Dv		latitude (topography-corrected) for each of the four vertices/corners (arranged counterclockwise starting at the trailing-left corner) of a 4-sided polygon that closely approximates the geolocated zone with the maximum TIRS image integration time
maxintgz_verts_lon	float32	3Dv		longitude (topography-corrected) for each of the four vertices/corners (arranged counterclockwise starting at the trailing-left corner) of a 4-sided polygon that closely approximates the geolocated zone with the maximum TIRS image integration time
orbit_phase_metric	float32	1D	degrees	orbit phase angular metric (range of 0-360 degrees, varying approximately linearly with time), defined as 0 deg at the ascending node (northward equator crossing) of the satellite orbit, 180 deg at the descending node, and so on
satellite_pass_type	int8	1D		flag specifying which type of satellite pass each frame is mostly/all part of. -1 = descending, 1 = ascending

### 2.2.5.2 *Atm* group

The *Atm* group contains all output from the clear-sky atmospheric retrieval, including prior and retrieved state information.

Table 2--4

Variable Name	Type	Dimension	Units	Description
cwv_prior	float32	2D	mm	column water vapor prior mean and first guess, derived from the Aux-Met product
cwv	float32	2D	mm	retrieved column water vapor
cwv_unc	float32	2D	mm	uncertainty of retrieval column water vapor

T_profile_prior	float32	3Dm	K	temperature profile prior mean and first guess derived from the Aux-Met product
T_profile	float32	3Dm	K	retrieved temperature profile
T_profile_unc	float32	3Dm	K	uncertainty of retrieved temperature profile
wv_profile_prior	float32	3Dm	g/kg	water vapor profile mean and first guess, derived from the Aux-Met product
wv_profile	float32	3Dm	g/kg	retrieved water vapor profile
wv_profile_log_unc	float32	3Dm		uncertainty of retrieved water vapor profile in log-space
wv_profile_unc	float32	3Dm	g/kg	uncertainty of retrieved water vapor profile
surface_T_prior	float32	2D	K	surface temperature prior mean and first guess derived from the Aux-Met product
surface_T	float32	2D	K	retrieved surface temperature
surface_T_unc	float32	2D	K	uncertainty of retrieved surface temperature
surface_pressure	float32	2D	hPa	surface air pressure
pressure_profile	float32	3Dn	hPa	pressure levels
altitude_profile	float32	3Dn	km	altitude levels
emissivity_prior	float32	3D		emissivity spectrum prior (over TIRS channels) used in the retrieval. Nominally taken from the 2B-Sfc product
posterior_covariance	float32	4D		posterior covariance output from optimal estimation algorithm
averaging_kernel_matrix	float32	4D		averaging kernel matrix output from optimal estimation algorithm
reduced_chi_squared_at_start	float32	2D		reduced chi squared at the first guess
reduced_chi_squared	float32	2D		reduced chi squared at the retrieved state
iterations	int8	2D		number of iterations
diverging_steps	int8	2D		number of diverging steps
atm_quality_flag	int8	2D		flag specifying the overall quality of the ATM retrieval for each scene (see Table 2-1 for details).
atm_qc_bitflags	uint16	2D		integer composed of bit flags that contain additional detail about the quality of the ATM retrieval/fields (see Table 2-2 for details).

### 3 Updates Since Previous Version

None – this is the initial version.

### 4 Known Issues

The effective information content of PREFIRE-TIRS measurements is strongly correlated with the amount of water vapor in the profile. This implies that the relative error grows with lower values of CWV. This behavior is important to recognize, particularly because the data of high scientific interest in the polar regions will often have low CWV. For further details on the algorithm implementation and results from retrievals of simulated data, consult the 2B-ATM ATBD and Miller et. al (2023).

The current version of the 2B-ATM algorithm uses the 2B-SFC product to set the surface spectral emissivity. Currently, the 2B-SFC values are used directly without modification, so errors in the emissivity may introduce error in the 2B-ATM retrieval. Note that if the 2B-SFC retrieval failed to produce values for a specific observation, the 2B-ATM algorithm will revert to a blackbody surface assumption (constant value of 1.0 emissivity). This condition is identified in *atm\_qc\_bitflags*.

The 2B-ATM algorithm runs in a similar configuration for all scenes for both PREFIRE-TIRS instruments and utilizes detector information in the 1B-RAD product to skip over bad pixels. This does imply that the quantitative atmospheric information content will have differences between scenes and instruments. These scene inconsistencies are not well understood within the early data. These inter-scene differences also impact the quality of the 2B-MSK product, which in turn means the observations retrieved by 2B-ATM will be statistically different populations across each scene. Utilizing a subset of data for R01 development testing (141 granules split across the first day of each month from July 2024 to February 2025) and given the quality assessment information described in section 2.2.3 we found that, on average, approximately 25% of all polar PREFIRE-SAT2 observations produce a QF = 0 "good quality" 2B-ATM retrieval. However, this fraction has some inconsistency, with a low of 20% (PREFIRE-TIRS2 Scene 7) and a high of 33% (PREFIRE-TIRS2 Scene 2). Note that on a granule basis, the fraction of good quality 2B-ATM ranged from ~5% to 50% of the polar data, depending on the cloudiness observed in any particular granule.

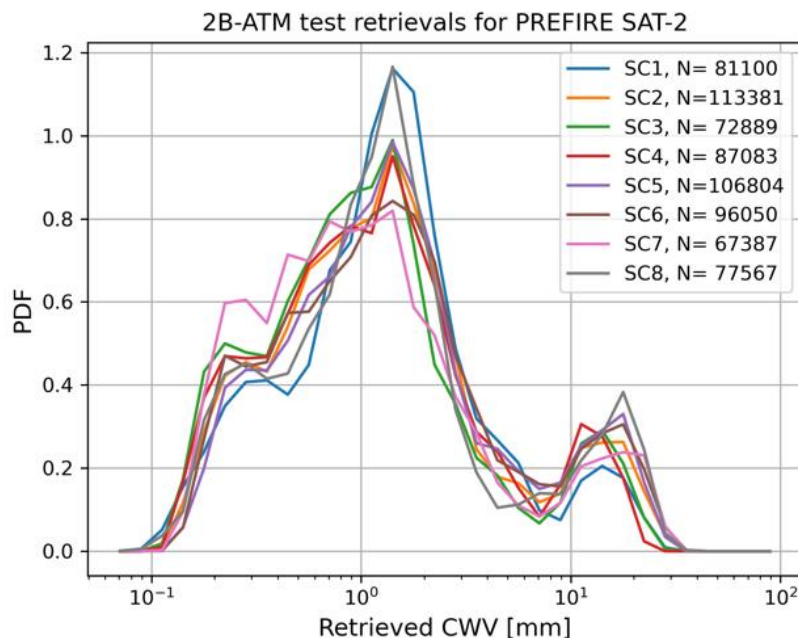


Figure 4-1. PDFs of the retrieved CWV from each PREFIRE-TIRS2 (on PREFIRE-SAT2) scene from within a set of 141 test granules. This is a large enough dataset that we expect the PDFs of each scene to be equivalent, and differences between scenes indicate inconsistencies in the radiometric signal and/or the retrieval performance. Some scene dependence is noted, particular at the high value "tail" of the distribution. Evaluating and minimizing these inter-scene biases will be a focus of future data releases.

#### *Geolocation:*

The GPS receiver on PREFIRE-SAT1 has performed poorly since launch, and the GPS receiver on PREFIRE-SAT2 ceased to function well at the end of August 2024. Because of the lack of continuously reliable GPS position and time data, the time-dependent orbital position and velocity vectors used for geolocation are based on orbital reconstructions. This uses publicly available orbit element sets (e.g., Two-Line Element sets (TLEs) based on ranging observations by the United States Space Force and other entities. The precision and accuracy of the orbit reconstruction is currently undergoing evaluation. In addition, residual uncertainties exist due to pointing offsets from lack of precise knowledge of the spectrometer slit orientation relative to the spacecraft. These uncertainties will be addressed after the orbit reconstruction is evaluated and optimized. The current best estimate is that individual geolocated scenes could have along-track geolocation errors of up to 50 km with an average of approximately 30 km (less than the along-track dimension of a ground footprint). The cross-track geolocation error has not been quantified, but the error is likely to be less than the cross-track scene width (approximately 12 km), based on favorable spatial correlations with co-located geostationary imagery collected in the MIR atmospheric window.

As more PREFIRE-TIRS data are collected and analyzed, the quantification of the geolocation biases will improve. Further refinements of the geolocation algorithm are planned, which will reduce these errors in future data product releases.

### *Electronic pattern noise:*

Electrical cross talk between adjacent FPA detectors was largely mitigated by alternating the wiring polarity in the readout integrated circuits. However, residual pattern noise has been noted in both the raw data and the calibrated radiances. This noise is highly temporally correlated and impacts all spectral channels.

This electrical noise manifests in two primary ways. First, “sawtooth-like” patterns can be visible in an individual spectral observation, where the even and odd spectral channels have different radiometric biases. These patterns are generally visible in spectral residuals (observation – modeled radiance). Due to the temporal correlation this pattern could be visible in multiple consecutive frames. Second, “striping” is visible when data from a selected channel are viewed spatially, where specific spatial scenes are clearly biased relative to the other scenes. Again, due to the temporal correlation these stripes will continue along track for some time. No data flagging is performed related to this pattern noise effect, but future developments in the calibration algorithm are planned to further reduce this noise.

## 5 Resources

The Algorithm Theoretical Basis Document (ATBD) can be found at [https://prefire.ssec.wisc.edu/Documents/PREFIRE\\_2B-ATM\\_ATBD.pdf](https://prefire.ssec.wisc.edu/Documents/PREFIRE_2B-ATM_ATBD.pdf). For more information, contact Erin Hokanson Wagner at [prefire-sdps.admin@office365.wisc.edu](mailto:prefire-sdps.admin@office365.wisc.edu).

## 6 References

Crisp, D., O’Dell, C., Eldering, A., Fisher, B., Oyafuso, F., et al., 2021. OCO (Orbiting Carbon Observatory)-2 Level 2 Full Physics Retrieval Algorithm Theoretical Basis, Tech. Rep. OCO D-55207, NASA Jet Propulsion Laboratory, California Institute of Technology, Pasadena, CA, Version 3.0 - Rev 1, available at:

[https://docserver.gesdisc.eosdis.nasa.gov/public/project/OCO/OCO\\_L2\\_ATBD.pdf](https://docserver.gesdisc.eosdis.nasa.gov/public/project/OCO/OCO_L2_ATBD.pdf) (last access: March 2025).

L’Ecuyer, T.S., Drouin, B.J., Anheuser, J., Grames M., Henderson, D., Huang, X., Kahn, B.H., Kay, J.E., Lim, B.H., Mateling, M., Merrelli, A., Miller, N.B., Padmanabhan, S., Peterson, C., Schlegel, N.-J., White, M.L., Xie, Y., “The Polar Radiant Energy in the Far-InfraRed Experiment: A New Perspective on Polar longwave Energy Exchanges,” *Bulletin of the American Meteorological Society (BAMS)*, 102(7), E1431–E1449, 2021.

Liu, X., Smith, W.L., Zhou, D.K., Larar, A., 2006. Principal component-based radiative transfer model for hyperspectral sensors: theoretical concept. *Appl. Opt.* 45, 201–209.

Miller, N. B., A. Merrelli, T. S. L'Ecuyer, and B. J. Drouin, 2023: Simulated Clear-Sky Water Vapor and Temperature Retrievals from PREFIRE Measurements. *J. Atmos. Oceanic Technol.*, **40**, 645–659, <https://doi.org/10.1175/JTECH-D-22-0128.1>.

Padmanabhan, S., Drouin, B., L'Ecuyer T., White, M., Lim. B., Kenyon, M., Mariani, G., McGuire J., Raouf, N., De Santos, O., Bendig, R., “The Polar Radiant Energy in the Far-InfraRed Experiment (PREFIRE),” *IGARSS 2019 – 2019 IEEE International Geoscience and Remote Sensing Symposium*

Rodgers, C. (2000) *Inverse Methods for Atmospheric Sounding: Theory and Practice*. World Scientific Publishing Co Pte. Ltd.

*Citation*

DOI:

- PREFIRE\_SAT2\_2B-ATM\_R01: 10.5067/PREFIRE-SAT2/PREFIRE/ATM\_L2B.R01
- PREFIRE\_SAT1\_2B-ATM\_R01: 10.5067/PREFIRE-SAT1/PREFIRE/ATM\_L2B.R01